RSC Advances

Formulation of Iron oxide particles using exopolysaccharide: Evaluation of their antibacterial and anticancer activity

Journal:	*RSC Advances*
Manuscript ID:	RA-ART-02-2015-003134.R1
Article Type:	Paper
Date Submitted by the Author:	03-Mar-2015

Complete List of Authors:	Venkatasamy, Vignesh; Bharathidasan University, Department of Animal Science Ganesan, Sathiyanarayanan; Bharathidasan University, School of Life Sciences G, Sathishkumar; Bharathidasan University, Department of Biotechnology and Genetic Engineering Karuppaiah, Parthiban; Bharathidasan University, Department of Animal Science K, sathishkumar; University of Aguascalientes, Ramasamy, Thirumurugan; Bharathidasan University, Animal Science

Cite this: DOI: 10.1039/c0xx00000x

www.rsc.org/xxxxxx

ARTICLE TYPE

Formulation of Iron oxide particles using exopolysaccharide: Evaluation of their antibacterial and anticancer activity

Venkatasamy Vignesh[a], Ganesan Sathiyanarayanan[b], Gnanasekar Sathishkumar[c], Karuppaiah Parthiban[a], Kamaraj Sathish Kumar[d] and Ramasamy Thirumurugan[a]*

Received (in XXX, XXX) Xth XXXXXXXXX 20XX, Accepted Xth XXXXXXXXX 20XX
DOI: 10.1039/b000000x

Abstract

In the present study, we report the formulation, characterization; in vitro antibacterial and cytotoxicity effect of exopolysaccharide (EPS) stabilized iron oxide nanoparticles (FeONPs) against epidermoid carcinoma cell line (A431). EPS is extracted from a spore forming strain VT03, *Bacillus subtilis* isolated from the gut microbiome of freshwater fish Oreochromis mossambicus (Tilapia). FTIR, 1H NMR and 13C NMR spectroscopic studies show the presence of sugar moieties confirming the EPS might be glucan. Later, EPS is used as an eco-friendly reducing and stabilizing agent for iron oxide nanoparticles (FeONPs) formulation. Initially, generation of nano scale FeO was confirmed through the formation of black colour precipitate with an absorbance maxima at 250-300nm in UV-Visible spectrometer. X-ray diffractogram (XRD) planes clearly confirm that the synthesized FeONPs are in the cubic spinel phase. Morphometric features of synthesized FeONPs are exclusively studied under electron Microscopy (FESEM and HRTEM) which displays spherical FeONPs in the size ranging between 75-120 nm, the mean size was found to be 106 ± 12 nm. Additionally, energy dispersive X-ray analysis (EDAX), selected area emission diffraction (SAED) and dynamic light scattering (DLS) authorizes the purity and homogeneity of synthesized FeONPs. Vibrating Sample Magnetometer (VSM) technique reveals the presence of both ferro and antiferromagnetic phases in EPS-stabilized FeONPs. Further, inhibitory activity of EPS-stabilized FeONPs against human and fish pathogenic strains like *Aeromonas hydrophila* (ATCC 49140), *Aeromonas hydrophila* (MTCC 1739), *Aeromonas sobria* (MTCC 3613) and *Aeromonas hydrophila* was assessed. *In vitro* cytotoxicity effect of free EPS and EPS-stabilized FeONPs were probed in epidermoid carcinoma cell A431. The IC_{50} value of EPS and EPS-stabilized FeONPs were found to be 350.18 and 62.946 µg/ml respectively. Further, Acridine orange/Ethidium bromide (AO/EtBr) staining of A431 cells at different time intervals clearly distinguishes the live cells and cells are undergone apoptotic cell death. In conclusion, our research paves a facile and greener route to synthesize FeONPs at room temperature. On the other hand, this study also proves that the formulated multifunctional hybrid FeONPs having stupendous qualities like enhanced bioavailability and magnetic properties. This can be developed into a successful theragnostic platform for cancer treatment.

KEYWORDS: *Bacillus subtilis*, Exopolysaccharide, Iron nanoparticles, antibacterial activity, antitumor activity.

1. Introduction

Exopolysaccharide (EPS) is long-chain branched polysaccharides having cyclical/repeated units of sugar moieties. The essence and significance of biopolymers in most of the sectors has made an urge to have more focus on EPS of microbes.[1] EPS can be either homopolymer (α-D-glucans, β-D-glucans, fructans and polygalactan)[2] or heteropolymer (D-glucose, D-galactose, L-rhamnose and, N-acetylglucosamine (GlcNAc), N-acetylgalactosamine (GalNAc) or glucuronic acid (GlcA)) based on linkage bonds and nature of monomeric units. Non-carbohydrate content may be present in few cases such as phosphate, acetyl and glycerol.[3] 1,4-β- or 1,3-β- linkages and 1,2-α- or 1,6-α- linkages can be found between monomeric units at the backbone of biopolymer.[4]

Bacteria synthesize polysaccharide using cell wall-anchored enzymes and secrete into the environment. Bacterial polysaccharide is said to be multifaceted which comprises of structural, intracellular and exopolysaccharides/extracellular polysaccharides. Homopolymer needs specific type of substrate

such as sucrose. The amount of exopolysaccharide production varies among of species of bacteria.[5] Complex EPSs are secreted by *Bacillus* spp. like *B. licheniformis*[6], *B. coagulans*, *B. polymyxa*[7], *B. megaterium*[8] and *B. mucilaginous.*[9] Previously, we report that EPS production by *Exiguobacterium* sp. Upon supplying sucrose in the medium components.[10] Among *Bacillus* spp, *Bacillus subtilis* strain is the unique one and foremost producer of EPS which acts as biofilm. It is found to produce the biopolymer poly-γ-Glutamate (PGA) [11, 12] and levan fructan by *Bacillus subtilis*.[13] Biofilm formation and EPS production in *Bacillus subtilis* are controlled by an operon of 15 genes.[14] Medium composition and physical parameters play a vital role in production of EPS, molecular size and composition.[15] Fish intestine is the most constructive ecological slot for microbiome, which attains more number of populations than water.[16] The use of spore forming bacteria like *Bacillus* sp. from indian carp *Oreochromis mossambicus* is more advantageous because of its survival and stability.

Formulation of nanoscale iron particles are of the current focus in nanoscience since they are being explored in the multiple applications like disinfection of water and remediation of heavy metals from polluted soils.[17,18] Although an array of synthesis using physical and chemical methods covering hydrothermal reaction, the sol-gel process, and chemical co-precipitation has been proposed, the same can be used for the formulation of iron oxide nanoparticles.[19] The synthesis of mono-dispersed nanoparticles with predetermined sizes and shapes has been a challenge in nanotechnology. Meanwhile, use of xenobiotic/toxic substrates as desizing/stabilizing agents during chemical synthesis limits their usage in biomedical applications, which is a major concern.[20] Therefore, it is a need of the hour to develop biocompatible, non-toxic and eco-friendly nanoparticle synthesis technologies which would be a boon to the scientific community and as well as for nano-industries. Although there are a number of ways to synthesize nanoparticles like certain reducing agents, as chemicals,[21,22] plant phytochemicals [23, 24 & 25] and microbial metabolites.[26, 27 & 28] Microbial synthetic route of metallic nanoparticles have become more important over other synthesis methods due to non-toxic to the environment and living things.[29]

In this context, most of the extracellular enzymes show excellent redox properties which act as an electron shuttle in the reduction of metal. Electron shuttles or other reducing agents like hydroquinones secreted by microorganisms are able to reduce ions into nanoparticles.[30] Some bacteria like *Mycobacterium paratuberculosis*[31], *Shewanella oneidensi*[32], *Geothrix fermentans*[33] were able to reduce Fe^{3+} oxides by producing and secreting small, diffusible redox compounds that can serve as an electron shuttle between the bacteria and the insoluble iron substrate.[34] Gold and silver nanoparticles have been synthesized by bacteria *B. subtilis* both extracellular and intracellular level.[35-38] Extracellular polymeric substances possess the hydroxyl groups, a hemiacetal reducing end and other functionalities which play important roles as both reducing and stabilizing/capping the inorganic nanoparticles.[39] However, the ability of extracellular polymeric secretion of this bacterium to formulate iron oxide nanoparticles is yet to be demonstrated and strengthened.

Even though EPS of Bacillus sp. is reported as an anticancer agent,[40] bioavailability is found to be less while considering biomedical applicaitons. Based on the gap in the area between extracellular secretions of bacteria and bioavailability, it is planned to investigate on one of the bacterial extracellular secretions like EPS for the formulation of iron oxide nanoparticles and its synergistic effect on cancer therapy. In order to explore the *Bacillus* sp. caliber of secreting useful metabolite like EPS from *Oreochromis mossambicus*, the present study was intended to screen a spore-forming strain *B. subtilis* for EPS production. The produced EPS was used as a reducing and stabilizing/capping agent for the formulation of FeONPs. Physico-chemical state of the formulated nanomaterials was exclusively characterized by adopting high throughput instrumentation like XRD, SEM, EDAX, TEM, DLS and VSM analyzes. An attempt was also taken to study the in vitro antibacterial activity against *Aeromonas* spp. and cytotoxicity studies of EPS-stabilized FeONPs in epidermoid carcinoma cell A431.

2. Experimental Sections

2.1 Screening of EPS producing bacteria

Herbivore, column feeder fish, Tilapia (*Oreochromis mossambicus*) was collected from Mokkombu (10°53'04.7"N 78°34'33.0"E), Cauvery river, Tiruchirappalli, Tamilnadu, India. To isolate potential bacilli group of microbiome, gastro intestinal tract was dissected out aseptically and homogenized in 0.89 % sodium chloride solution (10:1, volume: weight) using glass homogenizer. The homogenate was boiled at 100 ˚C for 5 min in order to isolate bacilli group.[41] Homogenate was serially diluted and plated on Bacillus agar (BA) medium (beef extract, 1.5g; yeast extract, 3g; pancreatic digest of casein, 3g; peptone, 6g; $MnSo_4$, 1µg; agar, 25g; distilled water, 1000 ml and pH: 7 ± 0.2) and incubated at 30˚C for 24 h. Morphologically 15 distinct colonies were screened for EPS production in nitrogen-deficient medium.[42] One of the strains (VT03) has shown positive for EPS production and the strain was designated as effective producer of EPS based on the productivity (data not shown). Selective strain VT03 was inoculated in 500 ml Erlenmeyer flask containing 150 ml of screening medium and incubated in an orbital shaker at 150 rpm for 72 h at 30˚C. After incubation, the cell-free supernatant (CFS) was collected and assessed for EPS productivity. All chemicals and reagents used in this present study were of analytical grade.

2.2 Identification of EPS producing bacteria

The strain VT03 was morphologically identified based on shape, motility, Gram and spore-staining and biochemical tests.[43, 44] The genomic DNA was isolated from VT03[45] and 16S rRNA sequences were amplified using universal primers of 27 F (AGAGTTTGATCMTGGCTCAG) and 1522 R (AAGGAGGTGATCCANCCRCA). A 50 µl volume of PCR reaction was performed using 10 ng of genomic DNA, 1× reaction buffer (10mM Tris-HCl at pH 8.8, 1.5mM $MgCl_2$, 50mM KCl, and 0.1% Triton X-100), 0.4mM (each)

deoxynucleoside triphosphates (Invitrogen), 0.5 U of DNA Polymerase (New England Labs, UK), and 1 mM of both forward and reverse primers. A PCR temperature profile of 94 ˚C for 1 min was used initially; then 30 cycles of 94 ˚C for 1 min, 52 ˚C for 1 min, 72 ˚C for 1 min and a final extension step at 72 ˚C for 10 min was performed. The various PCR products were cloned using the TOPO TA cloning kit based on the manufacturer's instructions (Invitrogen) for sequencing. The 16S rRNA gene sequence obtained from the VT03 was compared with the other bacterial sequences using NCBI mega BLAST (http://blast.ncbi.nlm.nih.gov/Blast.cgi) for their pair-wise identities. Multiple alignments of these sequences were carried out by Clustal W 1.83 version of EBI (www.ebi.ac.uk/cgi-bin/clustalw/) with a transition weight of 0.5. Phylogenetic tree was constructed using MEGA 5.0 version (www.megasoftware.net) by the neighbor joining (NJ), minimum evolution (ME), and unweighted pair group method along with the arithmetic mean (UPGMA) algorithms. Nucleotide composition of each aligned sequence was predicted by the BioEdit software package. The partial sequences of the 16S rRNA gene of the strain VT03 were submitted to NCBI GenBank.

2.3 Production, extraction and purification of EPS

In order to prepare the seed inoculum, culture medium containing glucose 15 g/L, yeast extract 0.6 g/L, KH_2PO_4 0.3 g/L, NaCl 0.1 g/L, $MgSO_4.7H_2O$, 0.4 g/L was prepared and inoculated with strain VT03. To produce EPS, 1000 mL Erlenmeyer flask containing 200 mL production medium (glucose 20 g/L, yeast extract 2.5 g/L, NH_4Cl 1.5 g/L, $MgCl_2$ 0.2 g/L, KH_2PO_4 1.0 g/L, K_2HPO_4 3.0 g/L, NaCl 1.5 g/L, pH 6.8 ± 0.2) was seeded with 20 mL of seed inoculum. The inoculated flask was incubated with 150 rpm agitation at 30 ˚C. Cell-free supernatant was obtained from cultured broth by centrifuging 200 ml of culture at 12 000× g for 10 min at 4 ˚C. Thermal treatment (80 ˚C, 1 h) was done to inactivate bacterial enzymes which might cause EPS degradation. Ice cold absolute ethanol was added into the cell-free supernatant at the ratio of 2 : 1 (v/v) and kept at 4 ˚C overnight to precipitate the exopolymeric substances. Centrifugation was performed at 14 000 × g for 15 min at 4 ˚C to collect the precipitate which was washed thrice with 70% ethanol-water mixtures. The precipitate was pooled together, dried in a desiccator and stored at 4 ˚C. EPS was re-dissolved in Milli-Q water and dialyzed overnight at 4˚C to remove salt contents. It was then lyophilized and stored at 37 ˚C. The lyophilized precipitate was dissolved in 50 mM phosphate buffer (pH-7.0) containing 0.5 M NaCl and purified through phenyl sepharose column (AKTA prime plus protein purification system, GE Healthcare, Sweden). The dissolved sample was eluted with the same buffer at the flow rate of 2 mL/min. The gel elution was lyophilized using freeze drier (Lark Innovative Fine Teknowledge, India) for further studies.

2.4 Characterization of EPS

Lyophilized crude EPS was dissolved in ultrapure Milli-Q water (0.1 g/L). The total carbohydrate,[46] protein,[47] and Sulfated sugars were determined.48 A 0.5 mg of purified EPS was mixed with potassium bromide (KBr) and dried and analysed by Fourier transform infrared spectrophotometer (FTIR) (Perkin Elmer, USA) with a resolution of 4 cm^{-1} in 4000-400 cm^{-1} region.[49] Nuclear magnetic resonance (NMR) spectra were obtained using a BrukerAvance 400 MHz spectrometer (Bruker Co., Billerica, MA) with a 5 mm inverse probe. EPS of the *B. subtilis* VT03 was dissolved in D_2O at concentrations of 5 mg/mL for ^1H NMR and in Dimethyl sulfoxide (DMSO)-d6 of about 20 mg/mL for ^{13}C NMR.

2.5 Formulation of iron nanoparticles (FeONPs) using EPS of bacterial strain VT03

The purified bacterial EPS of VT03 was collected as mentioned earlier and used for formulation of iron nanoparticles. About 2 mg/ml of EPS was added into the aqueous solution of 3M $FeCl_3$ (anhydrous) and 3M $FeSo_4$ dissolved in water in a mole ratio 2:3 of Fe^{3+}/Fe^{2+} in a 500 mL Erlenmeyer flask (pH 8.5-9). The mixture was then incubated at 35 ˚C (200 rpm) for 5 days under dark. A control setup was maintained without EPS. The flasks were tightly covered with aluminium foil in order to avoid photo reduction. The observations were recorded at every 12 h interval. The formulation of FeONPs was monitored by visual inspection of flask. The formulated nanoparticles were collected by high speed centrifugation (20 000 × g for 20 min), washed and dialyzed against Milli-Q water to get pure FeONPs.

2.6 Characterization of EPS-stabilized FeONPs

FeONPs was initially confirmed with the absorbance maxima in UV-visible spectroscopy. A small aliquot of sample was scanned with Perkin-Elmer Lambda 2 UV-visible spectroscopy at a wavelength ranging between 200 and 700 nm. The size of nanoparticles was analyzed with Malvern Zetasizer Nanoseries compact scattering spectrometer (Malvern Instruments Ltd., Malvern, UK). Further, core size and morphology of nanoparticles were examined under ZESIS FeSEM equipped with EDAX. Synthesized FeONPs were purified by ultracentrifugation at 30,000 rpm for 20 min to remove excessive ions and other debris; the resultant pellet was re-suspended in Milli-Q water and freeze dried and a thin film was prepared for FeSEM (ZESIS) analysis. The fine configuration of FeONPs was observed under high resolution transmission electron microscope (HRTEM) using (JEOL-JEM-200 CX). For the HRTEM measurements, a drop of the resulting solution was deposited on a copper-coated grid covered with amorphous carbon. In order to study the interaction of EPS with synthesized NPs, FTIR analysis was performed using (PerkinElmer Model RX1). The powdered samples mixed with KBr powder and pelletized were used for analysis, and the transmittance was recorded with wavelength ranging between 4000 cm^{-1} and 400 cm^{-1}. Crystallinity of sample was studied using an X-ray diffraction (XRD) system (PAN analytical X pert PRO Model) operated with Cu, Ka radiation at 40 kV and 30 mA. The magnetic properties of FeONPs under applied magnetic field of ± 1.5 Tesla were studied at room temperature (300 K) using Vibrating Sample Magnetometer (VSM) Model (Lake Shore-7474, USA)

2.7 Antibacterial activity

Non-repetitive strains of *Aeromonas hydrophila* (ATCC 49140), *Aeromonas hydrophila* (MTCC 1739), *Aeromonas sobria* (MTCC 3613) and *Aeromonas hydrophila* were maintained on tryptone soya agar and used to assess the inhibitory mechanism of formulated iron oxide nanoparticles. In brief, approximately 20

ml of nutrient agar medium was poured into sterilized petri dishes. The indicator organisms were grown in nutrient broth for 12 h. A 100 µl of nutrient broth culture of each bacterial strain (1 × 10^6 CFU/ml) was used to prepare bacterial lawns. Agar wells of 5 mm diameter were loaded with 100 µl of 100, 200, 300 and 400µg/ml Iron oxide nanoparticles (FeONPs). Acetic acid and distilled water were used as a positive and negative control, respectively. These plates were incubated at 37 ˚C for 24 h and then were examined for the presence of zone of inhibition. The diameter of such zone of inhibition was measured and the mean value for each organism was recorded and expressed in millimetre ± standard deviation (Mean ± SD).

2.8 *In vitro* anticancer property of EPS-stabilized FeONPs

2.8.1 MTT (3-(4,5-Dimethylthiazol-2-Yl)-2,5-Diphenyltetrazolium Bromide) assay

Epidermoid carcinoma cell line (A431) was procured from National Centre for Cell Science (NCCS), Pune, India. A431 cells were grown as monolayer in RPMI-1640 medium supplemented with 10% Fetal Bovine Serum, 1% glutamine, and 100 U/ml Penicillin-Streptomycin and incubated at 37 ˚C in 5% CO_2 atmosphere. Stocks were maintained in 75 cm^2 tissue culture flask. Cytotoxicity effect of synthesized FeONPs was measured using MTT assay. To execute MTT assay, briefly cultured A431 cells (1×10^6 cells/ml) were plated on 96 flat-bottom well plates, then cells were exposed to different concentration of filter sterilized EPS alone and EPS-stabilized FeONPs (10-500 µg/ml) and subsequently allowed for 24 h incubation at 37˚C in 5% CO_2 atmosphere. After incubation, 20 µl of MTT solution was added to each well and further incubated for another 4 h at 37 ˚C, and 5% CO_2 atmosphere. Finally, the formazan crystals were dissolved in 200 µl of DMSO and the absorbance was measured in a colorimetric at 570 nm with reference filter 630 nm with an ELISA reader (Bio-Rad Laboratories, CA, USA). Percentage of growth inhibition was determined using the formula: Growth inhibition % = {OD of control - OD of test/OD of control} × 100%, IC_{50} concentrations were determined as the concentration of EPS alone and EPS stabilized FeONPs required to fetch to half of the absorbance of control.

2.8.2 Biocompatibility assay of FeONPs

Hemolysis assay (*In vitro*) was performed. 5 ml of fresh blood was collected from healthy volunteer in a sterile glass vial containing EDTA. Red blood cells (RBCs) were separated by centrifugation of whole blood at 1500 rpm for 10 min. After discarding the supernatant containing plasma and platelets, the RBCs were washed thrice with sterile Phosphate buffered saline (PBS). Then, the pellets (1 ml) were resuspended in 3 mL of PBS. Then 0.1 ml of the diluted RBC suspension was added to 0.5 ml of the iron oxide nanoparticle suspension in PBS at an inhibitory concentration of 62.946 µg/ml in triplicate. The suspension was slightly vortexed and stored at static conditions for 4 h at 37^0C. Then, they were shortly vortexed again and centrifuged at 16000 rpm for 10 min. The above aqueous layer was measured for its absorbance value of haemoglobin at 575 nm by Perkin-Elmer Lambda 2 UV-V. A 0.1 ml of diluted RBC suspension incubated with 0.5 mL of water and 0.5 ml of PBS was used as a positive or negative control. The percentage of hemolysis was calculated using the formula: Hemolysis % = [(sample absorbance - negative control absorbance)/(positive control absorbance - negative control absorbance)] × 100%.[50-52]

2.8.3 Ao/EtBr staining of A431 cells treated with FeONPs

Cell death was measured by acridine orange/ethidium bromide staining. A431 cells were grown in six-well plates and treated with IC_{50} doses of EPS-stabilized FeONPs for 24 and 48 h. The culture medium containing the compound was removed and the cells were washed thrice with PBS, stained with 10 µl fluorescent dyes: acridine orange (AO)/ethidium bromide (EtBr) (100 µg, each/ml) for 5 min. The morphological changes in cells were observed by epi-fluorescence microscope (Carl Zeiss, Germany).

3. Results and Discussion

3.1 Screening and identification of EPS producing strain VT03

The freshwater fish intestine *Oreochromis mossambicus* facilitates an enormous source of bacterial community which produces valuable metabolites. The present study was aimed to isolate an exopolymeric substance producer from freshwater fish intestine. It revealed that the suspected strain VT03 was Gram-positive Bacilli, aerobic, endospore, motile rod and catalase positive. The optimum growth temperature was 35-37 ˚C with an optimal pH range of 6.5-7.5. The classifier programme of Ribosomal database project II(RDPII) (http://rdp.cme.msu.edu/) was used to retrieve taxonomic affiliation of the strain VT03 using 16S rRNA sequence. Phylogenetic tree (Fig. 1) was constructed using representative of maximum homologous (99%) sequences of the strain VT03 obtained from seqmatch programme of RDPII. VT03 was clustered with *Bacillus subtilis* GS1 and M50. RDPII search and phylogenetic analysis confirmed that the strain VT03 was *B. subtilis*. The 16S rRNA partial gene sequences of active producer VT03 was deposited in GenBank database with the assignment of accession number KC512905.

3.2 Characterization of EPS

The late log phase of bacterial growth facilitated the production of EPS by *Bacillus subtilis* (VT03). Cell density attained its maximum around 40 h of incubation. Chemical analysis revealed the composition of EPS from VT03 as carbohydrates, protein and sulfate in the concentration of 289.17, 111.43 and 25.12 mg/L, respectively. Carbohydrate content seems to be higher than other biomolecules.[53] The IR spectrum of pure EPS displays prominent transmittance at 3434, 1634, 1025 and 804 cm^{-1} corresponding to various functional groups present in the carbohydrate polymer (Fig. 5). The purified EPS consists of many hydroxyl groups like hydrogen bonded OH stretch frequencies, showing broad absorption peak around 3434 cm^{-1} characteristic of polysaccharide.[53] The stretching for carboxylic group was observed at 1634 cm^{-1}. The attributions for vibrations at 1025 and 804 cm^{-1} authorize that EPS isolated from *B. subtilis* VT03 is composed with sugar moieties connected with β-glycosidic linkages.[54] A peak at 1638 cm^{-1} was assigned to aromatic C-H stretch. The strong absorption peak at 1025 cm^{-1} depicting the aromatic C-H in plane bend corresponds to the presence of carbohydrates. Peak around 804 cm^{-1} gives clue about the presence of saccharide moieties.[42] 1-D ^{1}H NMR spectrum was obtained to identify the possible monosaccharide units, present in

the EPS. There were two specific protons (δ=~5.1 and ~4.6) (Fig. S2a) in the anomeric regions in the spectrum (δ=5.3 to 4.3). The observation of present study corraborates with the spectrum of glucan produced by *L. reuteri* confirming as glucopyranose.[55] In the 1D ^{13}C-NMR spectrum of the EPS, six carbon signals (104.05, 80.12,76.20, 75.36, 62.85, 60.49) were detected (Fig. S2b). A comparison with the ^{13}C NMR spectrum of the EPS with published chemical shifts of α-glucose, β-glucose[56], α-1, 4-glucan, and β-1, 6-glucan[57] demonstrate that the EPS might be glucan. The present observation was correlated with the outcomes of EPS produced by *Weissella hellenica*.[58]

3.3 Synthesis and Characterization of EPS stabilized FeONPs

The addition of EPS into the precursor Fe ion solution resulted in generation of FeONPs with a change in the color of reaction medium. Synthesized FeONPs exhibits blackish color due to the excitation of surface plasmonic vibrations[56] (Fig. 2a). Subsequently UV-visible spectrum of synthesized FeONPs produces a SPR peak at around 250 - 350 nm (Fig. 2b.), exhibiting the particles were stable and well dispersed in the solution.[60] Dynamic light scattering (DLS) size distribution intensity confirms the stability and dispersity of synthesized FeONPs in colloidal state. Stability of EPS-stabilized colloidal FeONPs solution has been investigated by Zeta potential (ζ), which is a measure of the electrostatic potential on the surface of the nanoparticle and is related to the eletrophoretic mobility of the colloidal suspension. Zeta potential of FeONPs was measured in the growth medium as -15.5 mV (Fig. S3a) and the surface of FeONPs was negatively charged (Fig. S3b), which provides the incipient instability (from ±10 to ±30mV) and the optimization experiments to increase the stability of EPS-stabilized FeONPs are currently in progress. Moreover, the hydrogen bonds present in the EPS provides a surface passivation against the agglomeration of FeONPs nanoparticles in aqueous and buffer solution.[42] X-ray diffraction patterns of biosynthesized FeONPs showed four distinct diffraction planes in the whole to (311), (400), (511) and (spectrum of 2θ values ranging from 30º to 70º. The interplanar distance were noticed at 2θ = 35.54º, 43º, 57º and 62.9º corresponds 440) Bragg reflection, respectively (Fig. 3). XRD pattern was analyzed and compared with the Joint Committee on Powder Diffraction Standards (JCPDS). It clearly shows that synthesized FeONPs were cubic spinel phase of magnetite and also highly matches with the standard magnetite XRD patterns.[61] As per Sherrer's equation, $D = k\lambda/B \cos\theta$ (20) the average grain size of nanoparticles was calculated as 110 nm. Electron microscopic studies (FESEM and HRTEM) shows spherical and polydispersed NPs with size ranging between 75-120 nm, the mean size was found to be 106 ± 12 nm. In particular, the HRTEM micrograph showed the fine configuration of synthesized FeONPs, a thin layer of EPS coating was noticed on the surface of FeONPs which act as stabilizing agent.[62] TEM analysis showed that FeONPs were synthesized inside of the bacterial exopolysaccharide matrix in the solution (Fig. 4a). The matrix was found to be isolated and some appeared as faint layered structures. The development of these faint layers may be due to the ionic interaction of iron with the surface functional groups like carboxylic group of the polymeric chain in the bacterial EPS. The size of the EPS complex formation depends on the interaction of the cation with the polymeric chain and on the ionic radii of iron. This complex structure of EPS along with cation can combine with other macromolecules in which cells and cell products may also be trapped.[63] As per the selected area electron diffraction analysis (SAED) synthesized FeONPs bestows the diffraction pattern of amorphous particles (Fig. 4b) which is reliable with many earlier reports.[64] Size distribution histogram was calculated from the HRTEM micrograph by measuring the diameters of around 50 particles using ImageJ software (Fig. 4c). However, within the aggregates of nanoparticles there is no contact between two particles were noticed, indicating the role of EPS as a capping and stabilization agent. The growth of iron nanocrystals (FeONPs) inside the EPS matrix may be because of the N-acetylated sugar molecules which are present in the EPS might have been acted as a reducing agent thereby reducing iron to iron nanocrystals. After the growth of iron nanocrystals they would have been entrapped in the complex matrix of polysaccharide. Hence, the synthesized nanoparticles would have been entrapped or encrusted into the EPS network responsible for the stabilization of FeONPs and, some of the nanoparticles were well dispersed and isolated. The bacterial EPS have N-acetylated amino sugars and also contribute for the adhesion process.[65] The size and shape of metallic nanoparticles depends on the concentration and type of reducing and stabilizing agents used. Experiments on how to control sizes and shapes of FeONPs synthesized with bacterial EPS are currently in progress. FESEM micrograph shows the aggregated topography of FeONPs (Fig. S1a), similar phenomenon was reported[60] where the SEM micrograph of iron oxide nanoparticles synthesized using EPS of *Bacillus subtilis* showed aggregates of particles with the size range between 60-80 nm. EDAX analysis stretches a strong elemental peak signal for Fe in the highest percentage confirming the purity of FeONPs (Fig. S1b). FTIR spectroscopic studies were performed to know the interaction between EPS and synthesized FeONPs. The FTIR spectrum of synthesized FeONPs (Fig. 5) showed variation in transmittance at different intensities due to the interaction of metal ion with EPS which leads to the reduction and stabilization of iron oxide nanoparticles. The intensities of transmittance at 3786.68, 3412.58, 2924.71, 1638.06, 1422.58, 1040.15 and 634.90 cm^{-1} were increased dramatically, whereas absorbance for β-glycosidic linkages at 804 cm^{-1} was found absent which proves the interaction of nanoparticles with this linkage. The band 634.90 cm^{-1} in between the region of 400 and 850 cm^{-1} revealed the presence of iron oxide nanoparticles. The bands at 1638.06 cm^{-1} and 3412.58 cm^{-1} attributes to the presence of carbonyl group (1,630 ~ 1,780 cm^{-1}) and organic functional group such as -NH or hydroxyl groups (3,200 ~3,600 cm^{-1}). A new peak was noticed at 1422.58 cm^{-1} owing to the oxidation of hydroxyl groups present in EPS.[66] In addition, the band at 1040.15 cm^{-1} represents the presence of C-O stretch in the region of 1,300 and 1000 cm^{-1} which might be due to the existence of covalent linking of ether or ester groups to the nanoparticles. The FTIR spectrum of FeONPs displayed the presence of carboxyl, hydroxyl and methoxyl groups and which were major groups of purified exopolysaccharide from strain *Bacillus subtilis* VT03 that could most possibly reduce the iron into nano scale FeO and stabilizing the nanoparticles in an aqueous solution. The electrostatic attractive forces between amino sugar moieties associated with

exopolysaccharide and Fe^{+} in solution afford an effectual driving force for the iron reduction and stabilization of the FeONPs. Therefore, in this report, we established that the green synthesis of FeONPs using bacterial exopolysaccharide and this approach is completely economic. Various plant-based polysaccharides were used for the synthesis and stabilization of different metallic nanocrystals,[67, 68] but bacterial polysaccharides have not yet been utilized for the synthesis of colloidal FeONPs.

The magnetic field dependence of magnetization at room temperature (RT) was carried out using VSM in the applied field range of ±15 KOe for FeONPs shown in Fig. 6. It is evident that at RT, the magnetic interactions of the sample are paramagnetic and also shows no saturation event at high magnetic field of 15 kOe, which implies the presence of both ferro and antiferromagnetic phases. The presence of the two types of magnetic phases is also confirmed from the non-symmetric hysteresis loop, as it is evident in the magnified loop given in the top left insert of Fig. 5. The shift towards negative direction is due to the exchange anisotropy and is known as exchange bias, HE.[69, 70] The coercivity (Hc) was found out as 87.58 Oe.

3.4 Antibacterial activity

The EPS-stabilized FeONPs revealed the potential to be bactericidal against four test strains of *Aeromonas* spp. causing ulcerative syndrome in freshwater fish (Table 1). As the concentration of FeONPs increases, the levels of inhibition of test strains are also being increased. Most of the researchers found that the levels of inhibition (bactericidal) are directly proportional to size of the nanoparticles.[71, 72] It could be due to the infiltration of the small particles into the cell membranes of bacteria.[73] There are several other mechanisms reported for the bactericidal activity of nanoparticles in which oxidative stress induced by reactive oxygen species (ROS) could be the most important consideration.[74,75] this can be explained that nano form of iron particles react with intracellular oxygen, followed by oxidative stress and subsequently inducing the disruption of the cell membrane.[76]

3.5 Anticancer property of EPS-stabilized FeONPs

MTT assay was carried out to assess the cytotoxic potential of EPS and EPS-stabilized FeONPs on human melanoma cell line A431 and to identify the IC_{50} values at 24 h. The present findings revealed that growth of A431 cells was significantly inhibited by both EPS alone and EPS-stabilized FeONPs in a dose-dependent manner. In particular, EPS-stabilized FeONPs showed significant growth reduction at 24 h. The IC_{50} concentration of EPS and EPS stabilized FeONPs were 350.18 and 62.946 µg/ml for 24 h treatment period (Fig. 7a).

Hemolysis is an outcome of a series of pathological conditions. To assess the biocompatibility, *in vitro* assay was performed to check the toxic nature of the EPS stabilized FeONPs. In this case, haemolytic activity of iron oxide nanoparticles on human melanoma cell line A431. As shown in Fig. 7b Compared to positive and negative control, haemolytic activity was less considerable implying its safe nature in application. In International Organization for Standardization/Technical Report 7406, the admissible level of hemolysis of biological based materials is 5%. The application of EPS stabilized FeONPs shows meagre level of hemolysis revealing their biocompatibility[50,52] and calibre for biomedical applications.[77] To find if there are any morphological features during apoptosis due to treatment of cells with EPS-stabilized FeONPs, acridine orange/ethidium bromide (AO/EtBr) fluorescent staining was used in treated and untreated A431 cells. As shown (Fig. 7c) untreated cells (control) did not show any morphological changes, indicated by the uniform green fluorescence, whereas cells treated with EPS-stabilized FeONPs showed significant morphological changes include chromatin condensation, cell shrinkage, vacuolation and apoptotic bodies formation at 12 and 24 h.

The most unique state is apoptotic cell death leading to the development of drugs for cancer. Classical pathway of cell death is a systematic and coordinated cellular mechanism for the elimination of cancer cells. In general, apoptosis is revealed by a sequence of morphological changes like shrinkage in the size of the nucleus and the cells, loss of adhesion to neighbour cells, condensation of chromatin, cell membrane blebbing and DNA fragmentation.[78] Eventhough, EPS has been reported for antitumour activity earlier. The large molecular size and hydrophilic property have decreased the biovailability of exopolysaccharides in biomedical applications.[79] In the present study, the synergistic use of EPS and FeONPs reveals more efficiency and increased bioavailability due to the properties of nanoparticles which is confirmed based on cytotoxicity study.

Conclusions

The fish intestine microbiome are interesting and yet to be explored. This is the first report mentioning the fish intestine associated bacterial strain as a potential source of EPS production. The study deals with feasible insight on bacterial metabolite EPS with significant caliber to reduce iron based materials. Thereby, the EPS conjugated iron nanomaterials facilitates the more bioavailabilty than EPS alone against epidermoid carcinoma cell line. It further makes the pavement towards anticancer agents and therapies in the clinical segments. Notably, EPS stabilized FeONPs unveiled the synergetic effect of anticancer activity at low IC_{50} value (62.946 µg/ml). The experimental results shows that bacterial EPS is responsible for the fabrication and stabilization of FeONPs and the EPS-stabilized iron nanocrystals could be used to treat bacterial infections, epidermoid cancer therapy and biomedical imaging.

Acknowledgements

The authors are also thankful to IIT SAIF for VSM technique, Pondicherry Centre for Biological Sciences for cytotoxicity study, UGC, UGC SAP DRS II for the instrumentation facility and DST FASTTRACK project for the financial support (Ref.No:SR/FT/LS-21/2012 dated 12.12.2012).

Notes and references

[a] *Laboratory of Aquabiotics/Nanoscience, Department of Animal Science, School of Life Sciences, Bharathidasan University, Tiruchirappalli - 620024, Tamil Nadu, India. Email: ramthiru72@gmail.com; Tel: +91-431-2407040; Fax: +91-431-2407045.*

[b]Department of Plant Science, School of Life Sciences, Bharathidasan University, Tiruchirappalli - 620024, Tamil Nadu, India
[c]Department of Biotechnology and Genetic Engineering, School of Life Sciences, Bharathidasan University, Tiruchirappalli - 620024, Tamil Nadu, India
[d]Engineering in Energy Department, Polytechnic University of Aguascalientes, CallePaseoSanGerardo No.207, Fracc. San Gerardo, Aguascalientes, Ags. C.P. 20342, Mexico

†

1 I. Bindhumol, K. M Nampoothiri, *Arch Microbiol*., 2010, 192, 1049-1057.
2 D.E.S. Stewart-Tull, *Annu. Rev. Microbiol*., 1980, 34, 311–340.
3 P. Ruas-Madiedo, J. Hugenholtz, P. Zoon, *Int. Dairy J*., 2002, 12, 163–171.
4 L. Martinez-Martinez, C. Timmerman, A. Fleer, J. Verhoef, *J. Med. Microbiol*., 1993, 39, 196–203.
5 D. Heumann, C. Barras, A. Severin, M.P. Glauser, A. Tomasz, *Infect Immun*., 1994, 62, 2715–2721.
6 A.E. Ghaly, F. Arab, N.S. Mahmoud, J. Higgins, *Am J Biochem Biotechnol*., 2007, 3: 47-54.
7 I.Y. Lee, W.T. Seo, G.J. Kim, M.K. Kim, S.G. Ahn, G.S. Kwon, Y.H. Park, *Bioprocess Eng*, 1997, 16: 71-75.
8 P. Himanshu Gandhi, M. Ramesh Ray, M. Rajni Patel, *Carbohydr Polym*., 1997, 34: 323-327.
9 B. Lian, Y. Chen, J. Zhao, H.H. Teng, L.J. Zhu, S. Yuan, *Bioresour Technol*., 2008, 99: 4825-4831.
10 Parthiban Karuppiah, Vignesh Venkatasamy and Thirumurugan Ramasamy, *International Journal of Oceanography and Marine Ecological System*., 2014, 3: 1-8.
11 Jane Yii Wu, Hsiu Feng Ye, *Process Biochem*, 2007, 42: 1114-1123.
12 Robert Mikutta, Ulrich Zang, Jon Chorover, Ludwig Haumaier, Karsten Kalbitz, *Geochim Cosmochim Acta*., 2011, 75: 3135-3154.
13 F.C.B. Cabral De Melo, D. Barsato, J.B. Buzato, M.A.P.C. Celligoi, *J Biotechnol*., 2010, 150S: S378.
14 K.P. Lemon, A.M. Earl, H.C. Vlamakis, C. Aguilar, R. Kolter, *Current Topics in Microbiology and Immunology*, 2008, 322: 1-16.
15 Chiu Yeh Wu, Zeng Chin Liang, Chiang Ping Lu, Shiu Hsiung Wu, *J Food Drug Anal*., 2008, 16: 61-67.
16 Austin, B., Austin, D.A, 1987. Ellis Horwood, Chichester, England. 364 p.
17 Q. Li, *Water Res*., 2008, 42, 4591-4602.
18 B.I. Kharisov, *RSC Adv*., 2012, 2, 9325-9358.
19 J. L. Dormann, L. Bessais, D. Fiorani, *J Physics*., 1988, 21, 2015-2034.
20 K. B. Narayanan, N. Sakthivel, *Adv Colloid Interface Sci*., 2010, 156, 1-13.
21 T. Siva Vijayakumar, S. Karthikeyeni, S. Vasanth, Arul Ganesh, G. Bupesh, R. Ramesh, M. Manimegalai, P.Subramanian, *J Nanosci*., 2013.
22 R. Ramesh, S. Arun, G. Rajagopal, P. Subramanian, M. Umadevi, R. Parimaladevi, N. Geetha, T. S. Geetha, Excel India Publishers; New Delhi, India., 2012, 28-29.
23 S. Karthikeyeni, T. Siva Vijayakumar, S. Vasanth, Arul Ganesh, M. Manimegalai, P. Subramanian, *J Acad Indus Res*., 2013, 10, 645-649.
24 V. Vignesh, K. Felix Anbarasi, S. Karthikeyeni, G. Sathiyanarayanan, P. Subramanian, R. Thirumurugan, *Colloids Surf A: Physicochem Eng Aspects*., 2013.
25 N. Kanipandian, R. Thirumurugan, Ind Crops Prod., 2014, 55, 1-10.
26 G. Sathiyanarayanan, G. S Kiran, J. Selvin, *Colloids Surf B*., 2013, 102, 13-20.
27 D. MubarakAli, J. Arunkumar, K. HarishNag, K.A. SheikSyedIshack, E. Baldev, D. Pandiaraj, N. Thajuddin, *Colloid Surf B*., 2012, 103, 166-173.
28 K. Sathish Kumar, R. Amutha, Palaniappan Arumugam, Sheela Berchmans, *ACS Appl Mater Interfaces*., 2011, 3, 1418-1425.
29 K. B. Narayanan, N. Sakthivel, *Adv Colloid Interface Sci*., 2010, 156, 1-13.
30 R. A. Baker, J. H. Tatum, *J Ferment. Bioeng*., 1998, 85, 359-361.
31 M. Homuth, P. Valentin-Weiganz, M. Rohde, G. F. Gerlach, *Infect Immu*., 1998, 66, 710-716.
32 D. P. Lies, M. E. Hernandez, A. Kappler, R. E Mielke, J. A. Gralnick, D. K. Newman, *Appl Environ Microbiol*., 2005, 71, 4414-4426.
33 K. P. Nevin, D. R. Lovley, *Appl Environ Microbiol*., 2002, 68, 2294-2299.
34 D. K. Newman, R. A. Kolter, *Nature*., 2000, 405, 94-97.
35 S. Minaeian, R. A. Shahverdi, S. A. Nohi, R. H. Shahverdi. *J Sci*. I.A., 2008, 17, 1-4.
36 T. J. Beveridge, R. G. E. Murray, *J Bacteriol*., 1976, 127, 1502-1518.
37 G. Southam, T. J. Beveridge, *Geochim Cosmochim Acta*., 1994, 58, 4227- 4230.
38 D. Fortin, T. J. Beveridge, Bäuerlein., Eds .;VCH: Germany., 2000 pp 7-24.
39 H. Huang, X. Yang, *Carbohydr Res*., 2004, 339(15), 2627-31.
40 K. Parthiban, V. Vignesh, R. Thirumurugan, *Afr J Biotechnol*., 2014, 13(21), 2137-2144.
41 K. Chantharasophon, T. Warong, P. Mapatsa, V. Leelavatcharamas, *Biotechnol*., 2011, 10, 498-505.
42 G. Sathiyanarayanan, V. Vignesh, G. Saibaba, A. Vinothkanna, K. Dineshkumar, M. B. Viswanathan, J. Selvin, *RSC Adv*., 2014, 4, 22817.
43 J. G. Holt, N. R. Kr1ly, P. H. A. Snlatil, J. T Stally, S. T. Williams, L. Williams, P. Wilkins, *Bergey's Manual of Determinative Bacteriology*., 1994, 562.
44 T. M. Barbosa, C. R. Serra, R. M. La Ragione, M. J. Woodward, A. O. Henriques, *Appl Environ Microbiol*., 2005, 71, 968-978.
45 C. Wawer, G. Muyzer, *Appl Environ Microbiol*., 1995, 61, 2203-2210.
46 M. Dubois, K. A. Gilles, J. K. Hamilton, P. A. Rebers, F. Smith, *Anal Chem*., 1956, 28, 350.
47 M. M. Bradford, *Anal Biochem*., 1976, 72, 248-254.
48 T. T. Terho, K. Hartiala, *Anal Biochem*., 1971, 41(2), 471-6.
49 X. Wang, J. F. Preston, T. Romeo, *J Bacteriol*., 2004, 186(9), 2724-34.
50 T. Yu, A. Malugin, H. Ghandehari, *ACS Nano*., 2011, 5(7), 5717.
51 M. A. Dobrovoiskaia, J. D. Clogston, B. W. Neun, J. B. Hall, A. K. Patri, S. E. McNeil, *Nano Lett*., 2008, 8, 2180.
52 P. V. Asharani, S. Sethu, S. Vadukumpully, S. P. Zhong, C. T. Lim, M. P. Hande, S. Valiyaveettil, *Adv Funct Mater*., 2010, 20, 1233.
53 Y. Wang, C. Li, P. Liu, Z. Ahmed, P. Xiao, X. Bai, *Carbohydr Polym*., 2010, 82, 895-903.
54 G. Raguenes, P. Pignet, G. Gauthier, A. Peres, R. Christen, *Appl Environ Microbiol*., 1996, 62, 67-73.
55 G. H. Van Geel-Schutten, E. J. Faber, E. Smit, K. Bonting, M. R. Smith, B. T. Brink, J. P. Kamerling, J. F. G. Vliegenthart, L. Dijkhuizen, *Appl Environ Microbiol*., 1999, 65, 3008-3104.
56 H.J. Kang, S.C. Baick, J. H. Yu, *Kor J Food Sci Ani Resour*., 2005, 25, 84-91.
57 I. Charkaraborty, M. Mondal, S. Pramanik, D. Rout, S. S. Islam, *Carbohydr Res*., 2004, 339, 2249-2254.
58 M. J. Kim, H. N. Seo, T. S. Hwang, S. H. Lee, D. H. Park, *J Microbiol*., 2008, 46, 535-541.
59 B. Kumar, K. Smita, L. Cumbal, A. Debut, *J Saudi Chem Soc*., 2014, 18, 364-369.
60 P. A. Sundaram, R. Augustine, M. Kannan, *Biotechnol Bioproc E*., 2012, 17, 835-840.
61 M. Mahdavi, F. Namvar, M. B. Ahmad, R. Mohamad, Extract. *Molecules*., 2013, 18, 5954-5964.
62 V. V. Makarov, S. S. Makarova, J. L. Andrew, O. V. Sinitsyna, O. Anna, I. V. Dudnik, M. Yaminsky, E. Taliansky, O. K. Natalia, *Langmuir*., 2014, 30, 5982−5988.
63 I.W. Sutherland, *Microbiol*., 2001, 147:3–9
64 V. Valentin Makarov, S. Svetlana Makarova, J. Andrew Love, V. Olga Sinitsyna, O. Anna Dudnik, V. Igor Yaminsky, E. Michael Taliansky, O. Natalia Kalinina, *Langmuir*., 2014, 30, 5982−5988.
65 S.E. Langille, G.G. Geesey, R.M. Weiner, *J Ind Microbiol Biotechnol*., 2000, 25 (2):81–85.
66 A.Mehta, C. Sidhu, A. K. Pinnaka, A. R. Choudhury, *Plos One*., 2014, 9 (6), 1-7.

67 B.Y. Park, Y. N. Hong, A. Weyers, Y. S. Kim, R. J. Linhardt, *Nanobiotechnol*., 2011, 5: 69.
68 B. Ankamwar, C. Damle, A. Ahmad, M. Sastry, *J Nanosci. Nanotechnol*., 2005, 5: 1665.
69 H. Shi, X. He, *J Phys Chem Solids*., 2012, 73: 646–650.
70 G.N. Rao, Y.D. Yao, J.W. Chen, *J Appl Phys*., 2009, 105: 093901/1–093901/6.
71 L. Zhang, Y. Jiang, Y. Ding, M. Povey, D. York, *J Nanopart Res*., 2007, 9 (3), 479-489.
72 S. Makhluf, R. Dror, Y. Nitzan, Y. Abramovich, R. Jelinek, A. Gedanken, *Adv Func Mater*., 2005, 15 (10), 1708-1715.
73 C. Lee, J. Y. Kim, W. I. Lee, K. L. Nelson, J. Yoon, D. L. Sedlak, *Environ Technol*., 2008, 42 (13), 4927-4933.
74 H. Sies, *Exp Physiol*., 1997, 82 (2), 291-295.
75 H. J. Park, J. Y. Kim, J. Kim, *Water Res*., 2009, 43 (4), 1027-1032.
76 J. S. Kim, E. Kuk, K. N. Yu, *Nanomed Nanotechnol Biol Med*., 2007, 3 (1), 95-101.
77 N.S. Rejinold, M. Muthunarayanan, V.V. Divyarani, P.R. Sreerekha, K.P. Chennazhi, S.V. Nair, *J Colloid Interface Sci*., 2011, 360: 39–51.
78 Y. W. Chen, C. F. Huang, C. Y. Yang, C. C. Yen, K. S. Tsai, S. H. Liu, *Toxicol Appl Pharmacol*., 2010, 243: 323-31.
79 Yi-Tao Chen, Qiang Yuan, Le-Tian Shan, Mei-Ai Lin, Dong-Qing Cheng, Chang-Yu Li, *Oncol Lett*., 2013, 5: 1787-1792.

Figure 1. Phylogenetic tree of the strain VT03 constructed by neighbour joining algorithm

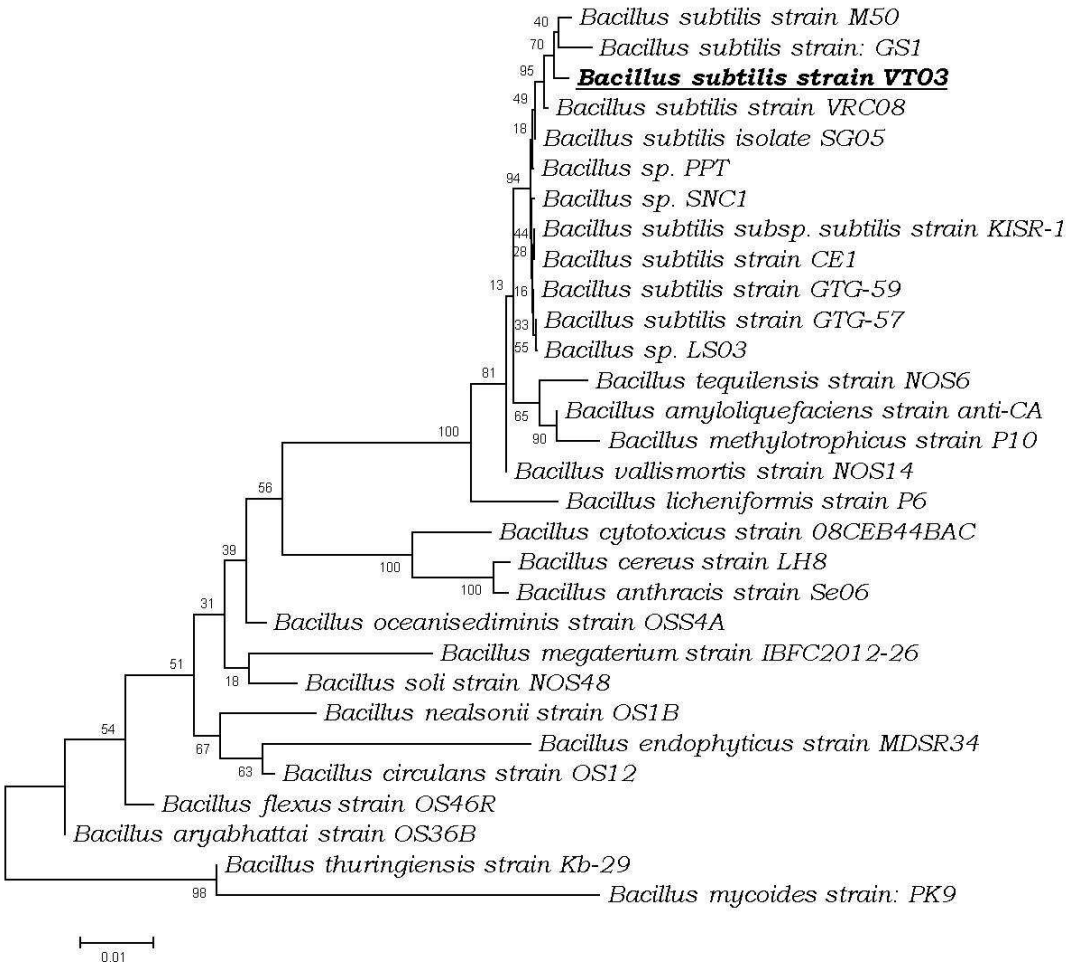

Figure 2a & b. UV-visible spectrum of the FeONPs

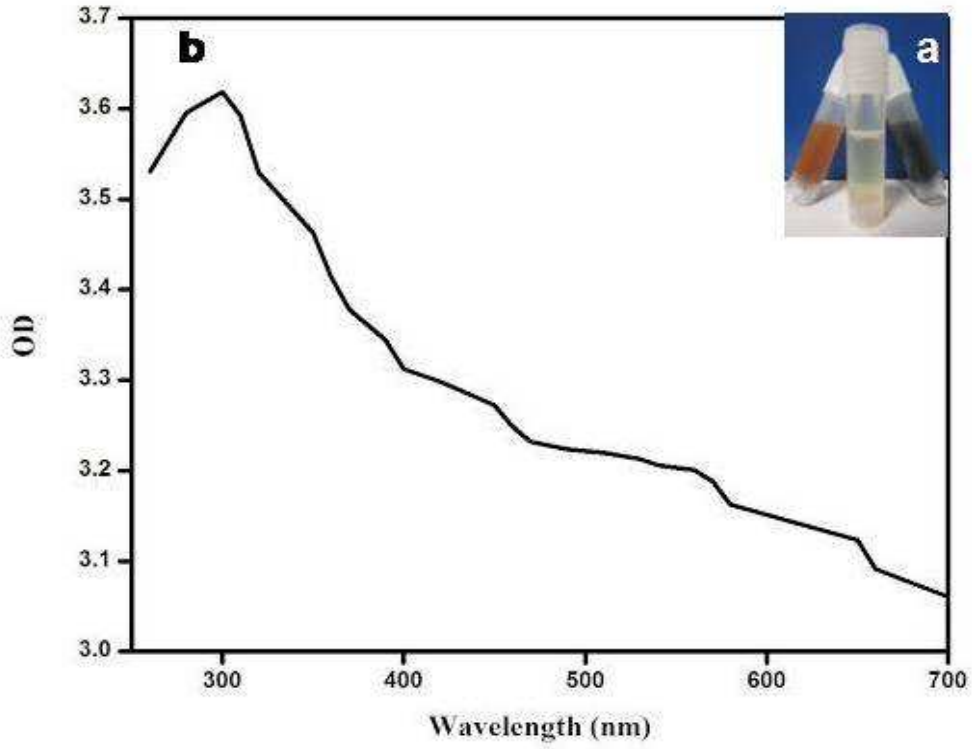

Figure 3. XRD diffractogram of FeONPs.

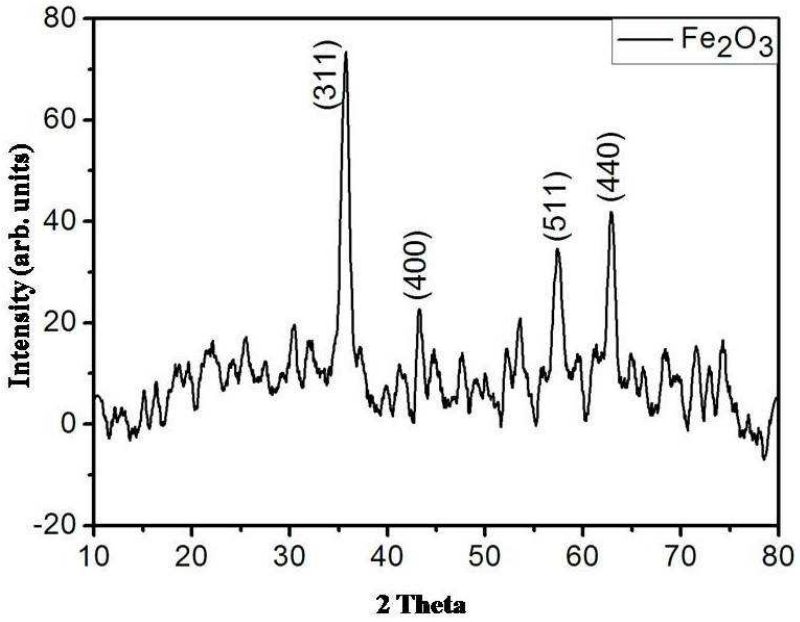

Figure 4. Morphometric studies of *FeONPs.*

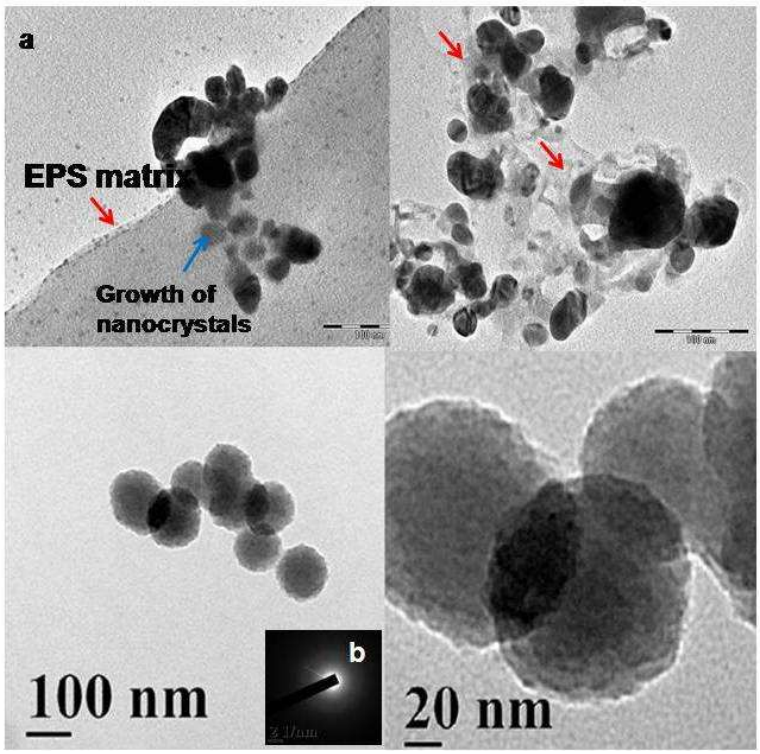

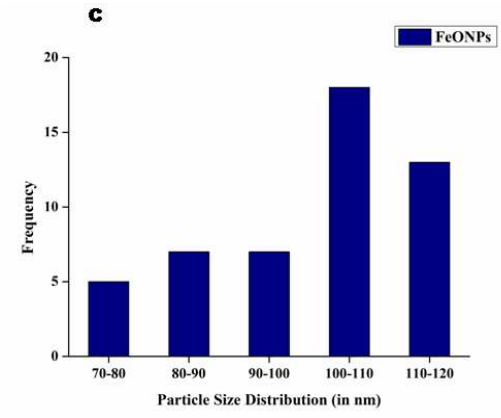

Figure 5. FTIR spectrum. a & b. Both synthesized *FeONPs* and EPS shows variation in the transmittance which is mainly due to the interaction of NPs with the functional group of EPS.

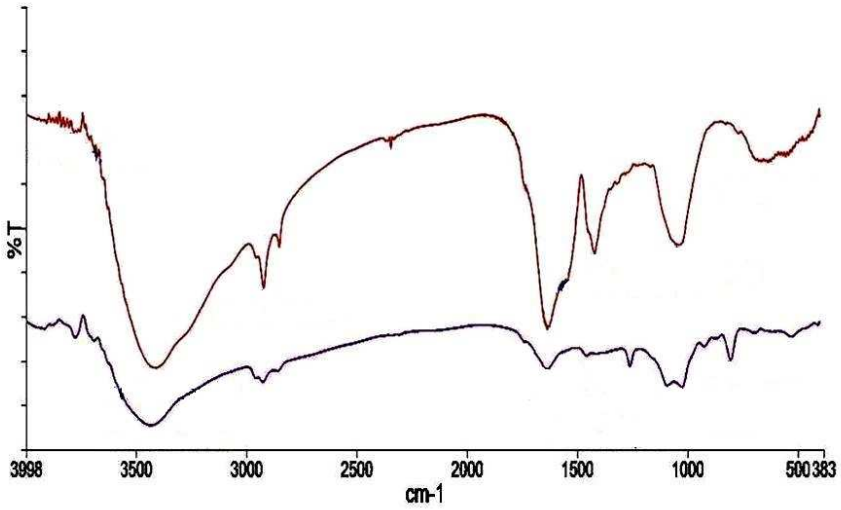

Figure 6. M(H) curves measured at 300 K for FeO nanoparticles. The insert shows the magnification of the central part of the M(H) curves at same temperature.

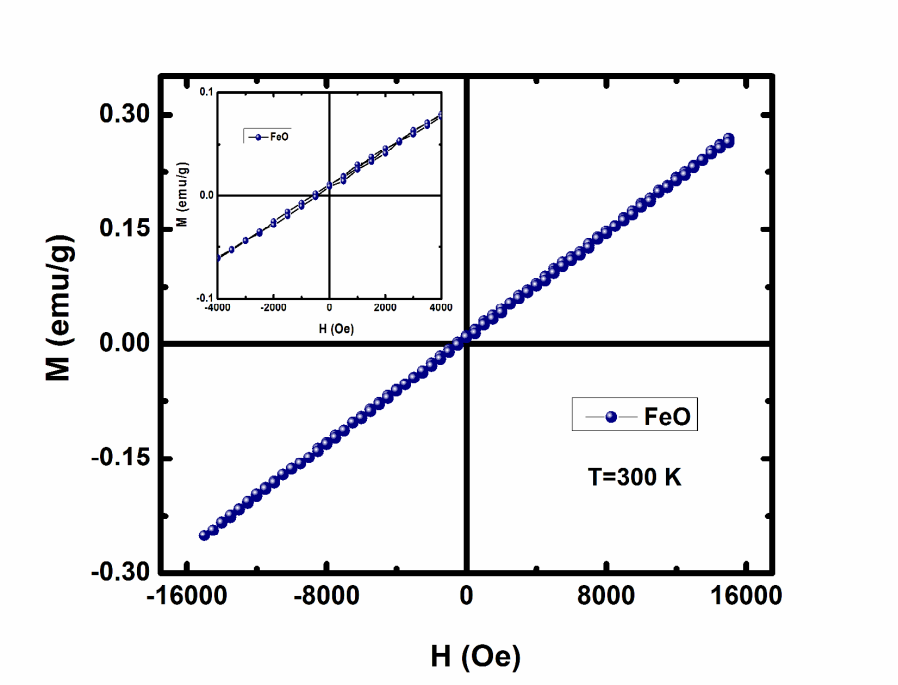

Figure 7a. MTT assay

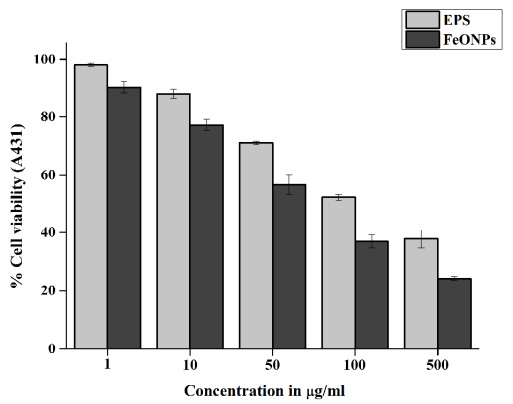

Figure 7b. *In vitro* Hemolysis assay

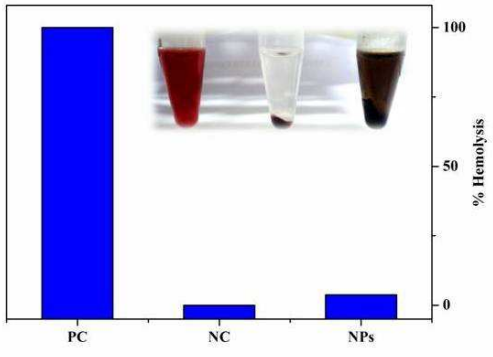

Figure 7c. AO/EtBr staining

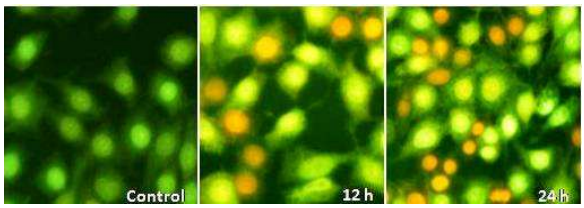

Table 1. Antibacterial activity of biosynthesized FeONPs

Test organism	Zone of inhibition (mm) by iron oxide nanoparticles in different concentrations (µg)			
	100	200	300	400
A.hydrophila	3.66 ± 1.5	5.66 ± 1.5	7.33 ± 0.5	7.66 ± 1.52
A.hydrophila	1.33 ± 0.5	2 ± 1	3 ± 1	5.33 ± 1.5
A.sobria	2.66 ± 1.5	3.33 ± 1.52	3.66 ± 2.08	2.33 ± 1.2
A.hydrophila	4.66 ± 1.52	2.66 ± 1.52	4.33 ± 1.2	4 ± 2

*All values are represented as Mean ± SD. The values are significant at $p < 0.05$ level